

## Interaction and ordering of lattice defects in oxygen-deficient rutile $\text{TiO}_{2-x}$

M. Aono

*The Institute of Physical and Chemical Research (RIKEN), Wako-shi, Saitama 351, Japan*

R. R. Hasiguti

*The Science University of Tokyo, Faculty of Engineering, Kagurazaka, Shinjuku-ku, Tokyo 162, Japan*

(Received 8 April 1993)

The atomic and electronic structures of lattice defects in oxygen-deficient rutile  $\text{TiO}_{2-x}$  ( $1 \times 10^{-4} \lesssim x \lesssim 3 \times 10^{-3}$ ) are discussed on the basis of electron-paramagnetic-resonance measurements. Titanium interstitials with a single paramagnetic electron ( $S = \frac{1}{2}$ ), which are the main lattice defects for small  $x$  ( $\lesssim 3 \times 10^{-4}$ ), strongly interact with each other for large  $x$  ( $\gtrsim 4 \times 10^{-4}$ ) resulting in Ti interstitial pairs with two paramagnetic electrons ( $S=1$ ) whose Ti-Ti distance and orientation are 3.25 Å and  $\langle 110 \rangle$ , respectively. At the same time, a considerable fraction of the Ti interstitials are ordered in cooperation with an oxygen deficit, resulting in  $\{121\}$  plane defects. The  $(121)$  plane defect contains Ti-ion pairs whose Ti-Ti orientation is  $\langle 100 \rangle$ , and the Ti-ion pair has two covalent-bond electrons and an additional paramagnetic electron ( $S = \frac{1}{2}$ ).

### I. INTRODUCTION

The lattice defects created in compounds by changing the composition of one of constituent elements from stoichiometry are of importance from both scientific and engineering points of view. In fact, such defects are often created in the processes of compound production and greatly affect the electric and mechanical properties of the compounds. However, the structures of such defects are often more complicated than one expects and it is not necessarily easy to analyze their structures. A good example is a certain defect in rutile ( $\text{TiO}_2$ ),<sup>1</sup> which is used in various electric and optical devices. By heating  $\text{TiO}_2$  in a reducing atmosphere, for example, its composition changes into oxygen-deficient  $\text{TiO}_{2-x}$ ; we shall consider the case of  $x \lesssim 3 \times 10^{-4}$  for a while. In much of the literature, the defects in oxygen-deficient  $\text{TiO}_{2-x}$  are simply regarded as oxygen (O) vacancies. Actually, however, the defects are titanium (Ti) interstitials as was critically reviewed in detail by Hasiguti.<sup>1,2</sup> Misunderstanding of this kind for various materials sometimes causes severe inconvenience in understanding and controlling the properties of the materials.

The present paper is concerned with lattice defects in oxygen-deficient  $\text{TiO}_{2-x}$  but deals with the case of larger  $x$ , i.e.,  $x \gtrsim 4 \times 10^{-4}$ . This work was initiated to clarify the electronic interaction among the above-mentioned Ti interstitials, which would affect the electronic properties of  $\text{TiO}_{2-x}$ . However, a more drastic interaction, i.e., the structural pairing of the Ti interstitials, has been found for a large part of the Ti interstitials by means of electron paramagnetic resonance (EPR). Furthermore, it has also been found by EPR that a large part of Ti interstitials are arranged orderly (in cooperation with O deficit) resulting in  $\{121\}$  plane defects. We have successfully analyzed the electronic structures of the Ti interstitial pair and the  $\{121\}$  plane defect. As is well known,<sup>3</sup> there is a series of

the "Magneli phases"  $\text{Ti}_n\text{O}_{2n-x}$  ( $n=4-9$ ), some of which exhibit interesting electric properties such as metal-semiconductor and semiconductor-semiconductor transitions. The crystal lattice of  $\text{Ti}_n\text{O}_{2n-1}$  (triclinic) can be constructed from that of  $\text{TiO}_2$  (tetragonal) by removing the  $(121)$  O plane every  $n$  planes and translating one side of the removed O plane relative to the other side by a vector of  $(0, 1/2, 1/2)$ . This  $(121)$  stacking fault in  $\text{Ti}_n\text{O}_{2n-1}$  is the same as the  $\{121\}$  plane defect in  $\text{TiO}_{2-x}$  mentioned above.

### II. EXPERIMENTAL

A single-crystal rod of  $\text{TiO}_2$  was cut into specimens with dimensions of  $12 \times 1 \times 1 \text{ mm}^3$ , their largest faces being parallel to  $(001)$  or  $(100)$ . The specimens were reduced into various oxygen-deficient compositions,  $\text{TiO}_{2-x}$  ( $1 \times 10^{-4} \lesssim x \lesssim 3 \times 10^{-3}$ ), by the following two methods. For small  $x$  ( $1 \times 10^{-4} \lesssim x \lesssim 3 \times 10^{-4}$ ), a specimen was put in an evacuated ( $8 \times 10^{-6}$  Torr) quartz capsule and heated at a high temperature in a temperature-controlled electric furnace. In this case,  $x$  could be controlled by changing the volume of the capsule and the heating temperature (1000–1400°C). For large  $x$  ( $3 \times 10^{-4} \lesssim x \lesssim 3 \times 10^{-3}$ ), a specimen was placed at a closed end of a quartz tube and heated at a high temperature with the other end of the tube being continuously evacuated ( $8 \times 10^{-6}$  Torr). In this case,  $x$  could be controlled by changing the heating temperature (1000–1400°C). The value of  $x$  was measured with the following two methods. One is to measure a weight loss (and a weight gain after reoxidation into  $\text{TiO}_2$ ) with a high-precision microbalance. This method was not useful for small  $x$ , so that the amount of oxygen built up in the capsule was measured by breaching the capsule in a specially designed oil manometer. The values of  $x$  measured in these different methods agreed reasonably well in an

overlapping region. It should be mentioned that, in order to obtain homogeneous single-crystal specimens of  $\text{TiO}_{2-x}$  with large  $x$ , it took more than 1000 h in heating time.

All EPR measurements were made at 4.2 K with an X-band spectrometer (JEOL JES-3) operated at a microwave frequency of 9.214 GHz. The calibration of the external magnetic field was made by using a standard sample, DPPH.

### III. RESULTS AND DISCUSSION

Figure 1 shows a typical EPR spectrum of  $\text{TiO}_{2-x}$ , which was measured for a specimen with  $x = 5 \times 10^{-4}$  at 4.2 K with the external magnetic field parallel to [001]. The spectrum consists of three spectra "C", "X," and "W" as indicated; the naming of the spectra will be described later.

In this paper, the "C" spectrum, which was found and named by Chester,<sup>4,5</sup> will not be discussed in detail since it was already analyzed by Hasiguti<sup>2</sup> and identified to be due to a Ti interstitial with a single paramagnetic electron; this identification was later confirmed by Yagi *et al.*<sup>6</sup> with proton channeling experiments. However, for our later discussion, it is necessary to give a brief interpretation about the "C" spectrum.

#### A. The "C" spectrum

The "C" spectrum has the same origin as the "A" spectrum (not seen in Fig. 1) that was also found and named by Chester,<sup>4,5</sup> as discussed by Hasiguti.<sup>2</sup> Namely, both the "C" spectrum and the "A" spectrum are due to a Ti interstitial with a single paramagnetic electron. If the concentration of the Ti interstitial is small enough, they give the "A" spectrum consisting of four resonance lines, but as the concentration increases, the "A" spectrum changes into the "C" spectrum consisting of single resonance lines owing to exchange narrowing. Because of this, the "A" spectrum contains more detailed informa-

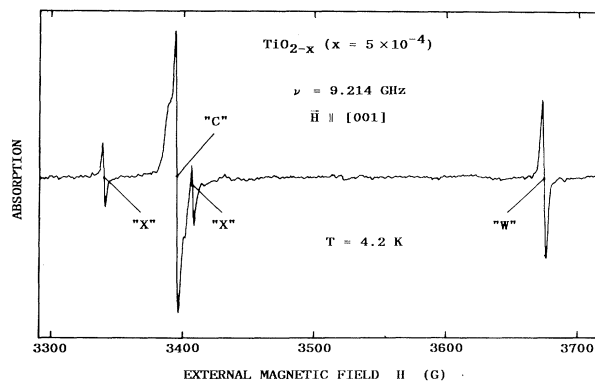


FIG. 1. EPR spectrum of  $\text{TiO}_{2-x}$  with  $x = 5 \times 10^{-4}$  measured at 4.2 K with the external magnetic field being swept in the [001] crystal axis. The frequency of electromagnetic wave was 9.214 GHz. The shoulders on the both sides of the main resonance line of the "C" spectrum are a hyperfine structure, which is not well resolved because of exchange narrowing.

tion on the Ti interstitial rather than the "C" spectrum. The principal axes and principal values of the  $\underline{g}$  tensor in the effective spin Hamiltonian

$$H = \beta \mathbf{H} \cdot \underline{g} \cdot \mathbf{S} \quad (1)$$

(the notations have usual meanings) of the single paramagnetic electron ( $S = \frac{1}{2}$ ) of the Ti interstitial are determined from the resonance magnetic fields of the "A" spectrum plotted against the direction of the external magnetic field shown in Figs. 2(a) and 2(b) by broken lines (remeasured in the present work) and the results are shown in Table I. As we see in Table I, the principal axes of the  $\underline{g}$  tensor in the (001) plane are deviated from the [100] and [010] crystal axes by  $26^\circ$ . The position of the Ti interstitial, which was analyzed by Hasiguti<sup>2</sup> on the basis of similar experiments, is shown in Fig. 3. This position is consistent with the principal axes shown in Table I since the symmetry axes of the octahedron of O

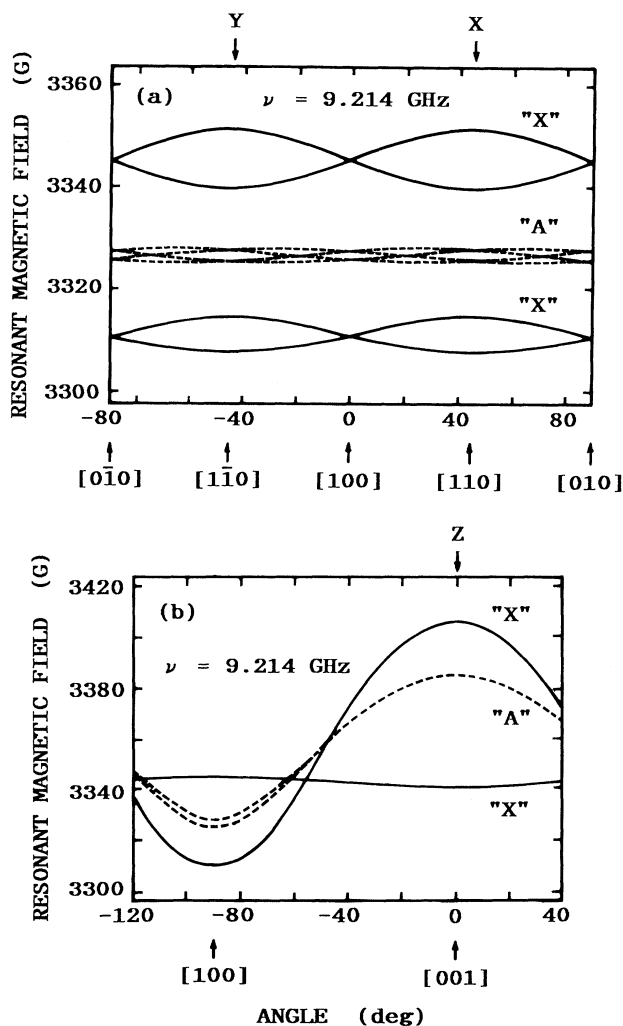


FIG. 2. Resonant magnetic fields of the "A" (dashed lines) and "X" (solid lines) spectra plotted against the direction of the external magnetic field. The measurements were made at 4.2 K with an electromagnetic wave of 9.214 GHz.

TABLE I. Principal axes and principal values of the  $g$  tensor of the "A" spectrum.

Principal axis	Principal value
[001] ( $\xi$ )	1.9414 ( $g_\xi$ )
[100] $\pm 26^\circ$ ( $\eta$ )	1.9780 ( $g_\eta$ )
[010] $\pm 26^\circ$ ( $\zeta$ )	1.9746 ( $g_\zeta$ )

ions surrounding the Ti interstitial are rotated in the (001) plane by  $32^\circ$ , which is close to  $26^\circ$ , from the  $\langle 100 \rangle$  crystal axes as indicated in Fig. 3(b); the small difference between the two angles ( $32^\circ$  and  $26^\circ$ ) is not serious because the crystal field at the Ti interstitial is created not only by the nearest O ions but by the next-nearest Ti ions, as will be discussed later.

As for the charge state of the Ti interstitial, there are two possibilities of  $Ti^{3+}$  and  $Ti^{1+}$  because of its electron spin of  $S = \frac{1}{2}$ . We prefer  $Ti^{3+}$ , according to an EPR study of the "A" spectrum by Kingsbury, Ohlsem, and Johnson.<sup>7</sup> The spatial distribution of the paramagnetic electron of the  $Ti^{3+}$ , however, seems to be considerably larger than that of  $Ti^{1+}$  in usual complex salts of titanium. In fact, in the latter case, the principal axes of the  $g$  tensor are almost completely determined by the crystal field of the nearest O ions,<sup>8</sup> whereas the paramagnetic electron of the  $Ti^{3+}$  of concern feels an additional crystal field of the next-nearest Ti ions to a considerable extent, as already described. The interstitial  $Ti^{3+}$  is a donor center and its ionization energy is  $5 \times 10^{-3}$  eV as mea-

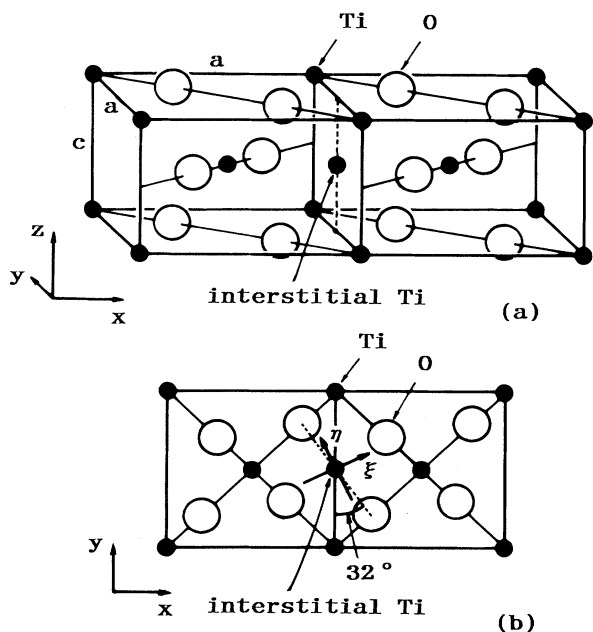


FIG. 3. (a) Three-dimensional view and (b) its two-dimensional projection of the lattice of  $TiO_2$  containing a Ti interstitial. The principal axes of the  $g$  tensor of a paramagnetic electron ( $S = 1/2$ ) trapped by the Ti interstitial are denoted by  $\xi$ ,  $\eta$ , and  $\zeta$  ( $\zeta$  is not shown explicitly but perpendicular to  $\xi$  and  $\eta$ ).

sured from the temperature dependence of electrical conductivity.<sup>9</sup> This small ionization energy is consistent with what was mentioned above.

We can now discuss the origins of the "X" and "W" spectra in Fig. 1 on the basis of the brief interpretation of the "A" spectrum given above.

### B. The "X" Spectrum

The "X" spectrum was found and named by Hasiguti and co-workers<sup>9,10</sup> in their preliminary study. The "X" spectrum consists of four resonance lines and their resonance magnetic fields vary against the direction of the external magnetic field as shown in Figs. 2(a) and 2(b) by solid lines. As we see in Fig. 2(b), the "X" spectrum splits into two resonance lines even in the principal symmetry axis of  $TiO_2$  [001], and the behavior observed in Fig. 2(b) is typical of a paramagnetic center of  $S = 1$ . Therefore, we shall analyze the "X" spectrum with the following effective spin Hamiltonian for  $S = 1$ :

$$H = \beta \mathbf{H} \cdot \mathbf{g} \cdot \mathbf{S} + \mathbf{S} \cdot \mathbf{D} \cdot \mathbf{S} \quad (2)$$

(the notations have usual meanings). The principal axes

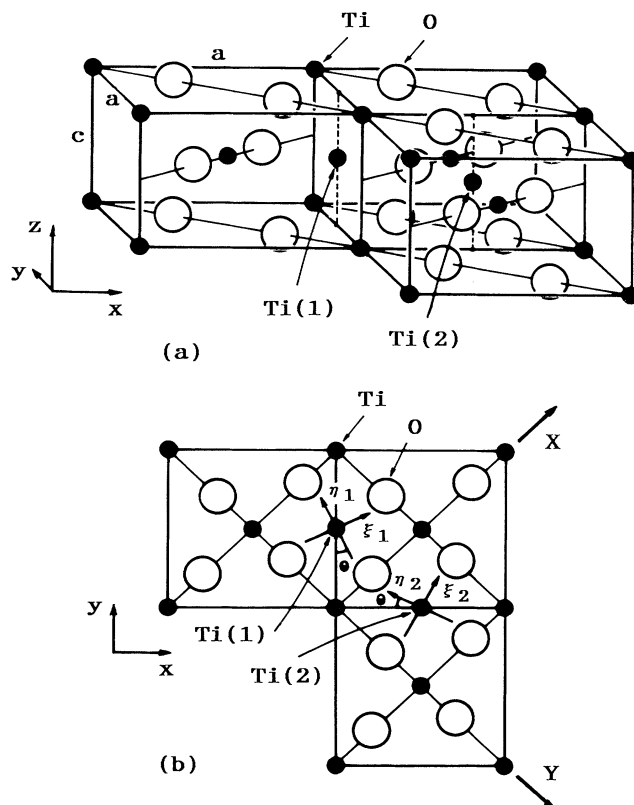


FIG. 4. Three-dimensional view (a) and its two-dimensional projection (b) of the lattice of  $TiO_2$  containing a Ti interstitial pair  $Ti(1)$ - $Ti(2)$ .  $\xi_1$ ,  $\eta_1$ , and  $\zeta_1$  for  $Ti(1)$  and  $\xi_2$ ,  $\eta_2$ , and  $\zeta_2$  for  $Ti(2)$  correspond to  $\xi$ ,  $\eta$ , and  $\zeta$  in Fig. 3, respectively ( $\zeta_1$  and  $\zeta_2$  are not shown explicitly but perpendicular to  $\xi_1$  and  $\eta_1$  on one hand and  $\xi_2$  and  $\eta_2$  on the other hand, respectively).  $X$ ,  $Y$ , and  $Z$  show a coordinate system used in the analysis of the interaction between two paramagnetic electrons trapped by  $Ti(1)$  and  $Ti(2)$  ( $Z$  is not shown explicitly but perpendicular to  $X$  and  $Y$ ).

and principal values of the  $\underline{g}$  and  $\underline{D}$  tensors, which are found from Figs. 2(a) and 2(b), are shown in Table II.

We have examined a number of possible origins of the "X" spectrum and found that the "X" spectrum is due to a pair of Ti interstitials shown in Fig. 4, where Ti(1) and Ti(2) indicate two equivalent Ti interstitials, each of which is essentially the same as the Ti interstitial discussed above. The Ti(1)-Ti(2) distance and orientation are 3.25 Å and  $\langle 110 \rangle$ , respectively. The pair of Ti(1) and Ti(2) is fully consistent with our experimental results for the "X" spectrum shown in Figs. 2(a) and 2(b) and Table II as follows (we will describe the analysis in detail because it will be necessary for our later discussion).

The principal axes and principal values of the  $\underline{g}$  tensor for Ti( $i$ ) ( $i=1,2$ ) will be denoted by  $\xi(i)$ ,  $\eta(i)$ , and  $\zeta(i)$  on one hand and  $g_{\xi(i)}$ ,  $g_{\eta(i)}$  and  $g_{\zeta(i)}$  on the other hand, respectively. Namely, the  $\underline{g}$  tensor for Ti( $i$ ) is expressed as

$$\underline{g}_{[\xi(i), \eta(i), \zeta(i)]}^{(i)} = \begin{bmatrix} g_{\xi(i)}^{(i)} & 0 & 0 \\ 0 & g_{\eta(i)}^{(i)} & 0 \\ 0 & 0 & g_{\zeta(i)}^{(i)} \end{bmatrix} \quad (3)$$

in its principal-axis coordinate system. We tentatively assume that the principal axes and principal values of  $\underline{g}^{(1)}$  and  $\underline{g}^{(2)}$  are the same as those of the  $\underline{g}$  tensor for the isolated Ti interstitial given in Table I. Namely,

$$g_{\xi(1)}^{(1)} = g_{\xi(2)}^{(2)} = g_{\xi} \quad (=1.9414), \quad (4)$$

$$g_{\eta(1)}^{(1)} = g_{\eta(2)}^{(2)} = g_{\eta} \quad (=1.9780), \quad (5)$$

$$g_{\zeta(1)}^{(1)} = g_{\zeta(2)}^{(2)} = g_{\zeta} \quad (=1.9746). \quad (6)$$

If we express (3) in the  $X$ ,  $Y$ , and  $Z$  coordinate system shown in Fig. 4(b), we obtain

$$\underline{g}_{(X, Y, Z)}^{(1)} = \begin{bmatrix} a & d & 0 \\ d & b & 0 \\ 0 & 0 & c \end{bmatrix}, \quad (7)$$

TABLE II. Principal axes and principal values of the  $\underline{g}$  and  $\underline{D}$  tensors of the "X" spectrum.

Principal axis	$\underline{g}$ tensor	
	Principal value	
[001] ( $Z$ )	1.9509	
[110] ( $Y$ )	1.9802	
[1 $\bar{1}$ 0] ( $X$ )	1.9846	
$\underline{D}$ tensor		
[001] ( $Z$ )	$1.9 \times 10^{-3} \text{ cm}^{-1}$	
[110] ( $Y$ )	$-0.9 \times 10^{-3} \text{ cm}^{-1}$	
[1 $\bar{1}$ 0] ( $X$ )	$-1.0 \times 10^{-3} \text{ cm}^{-1}$	

$$\underline{g}_{(X, Y, Z)}^{(2)} = \begin{bmatrix} a & -d & 0 \\ -d & b & 0 \\ 0 & 0 & c \end{bmatrix}, \quad (8)$$

where

$$a = g_{\xi} \cos^2 \theta + g_{\eta} \sin^2 \theta, \quad (9)$$

$$b = g_{\xi} \sin^2 \theta + g_{\eta} \cos^2 \theta, \quad (10)$$

$$c = g_{\zeta}, \quad (11)$$

$$d = (g_{\xi} - g_{\eta}) \sin \theta \cos \theta, \quad (12)$$

$\theta$  being the angle shown in Fig. 4(b), which is  $26^\circ$  according to Table I.

We can write the spin Hamiltonian of the pair of Ti(1) and Ti(2) as

$$H = \beta \mathbf{H} \cdot \underline{g}^{(1)} \cdot \mathbf{S}^{(1)} + \beta \mathbf{H} \cdot \underline{g}^{(2)} \cdot \mathbf{S}^{(2)} + \mathbf{S}^{(1)} \cdot \mathbf{J} \cdot \mathbf{S}^{(2)}, \quad (13)$$

where the first and second terms represent the Zeeman interactions of the paramagnetic electrons of Ti(1) and Ti(2), respectively, and the third term represents the exchange interaction between the two paramagnetic electrons. If we express (13) in the  $X$ ,  $Y$ , and  $Z$  coordinate system using (7) and (8), we obtain

$$H = \beta [H_X(S_X^{(1)}a + S_Y^{(1)}d) + H_Y(S_X^{(1)}d + S_Y^{(1)}b) + H_Z S_Z^{(1)}c + H_X(S_X^{(2)}a + S_Y^{(2)}d) + H_Y(-S_X^{(2)}d + S_Y^{(2)}b) + H_Z S_Z^{(2)}c] + J_X S_X^{(1)} S_X^{(2)} + J_Y S_Y^{(1)} S_Y^{(2)} + J_Z S_Z^{(1)} S_Z^{(2)}. \quad (14)$$

When  $\mathbf{H}$  is parallel to  $Z$ , (14) is reduced to

$$H = \beta H_Z c (S_Z^{(1)} + S_Z^{(2)}) + J_Z S_Z^{(1)} S_Z^{(2)} + \frac{1}{4} (J_X - J_Y) S_+^{(1)} S_+^{(2)} + \frac{1}{4} (J_X + J_Y) S_+^{(1)} S_-^{(2)} + \frac{1}{4} (J_X + J_Y) S_-^{(1)} S_+^{(2)} + \frac{1}{4} (J_X - J_Y) S_-^{(1)} S_-^{(2)} \quad (15)$$

if  $Z$  is taken to be the quantization axis, where the subscripts  $+$  and  $-$  indicate the up and down spins, respectively. As the basis of the representation of (15), we take state vectors  $|+\frac{1}{2}, +\frac{1}{2}\rangle$ ,  $|-\frac{1}{2}, -\frac{1}{2}\rangle$ ,  $|+\frac{1}{2}, -\frac{1}{2}\rangle$ , and  $|-\frac{1}{2}, +\frac{1}{2}\rangle$ , where  $i$  and  $j$  in  $|i, j\rangle$  are the spin quantum numbers of the paramagnetic electrons of Ti(1) and Ti(2), respectively. In this case, (15) is represented as

$$H = \begin{bmatrix} \beta H_Z c + J_Z/4 & (J_X - J_Y)/4 & 0 & 0 \\ (J_X - J_Y)/4 & -\beta H_Z c + J_Z/4 & 0 & 0 \\ 0 & 0 & -J_Z/4 & (J_X + J_Y)/4 \\ 0 & 0 & (J_X + J_Y)/4 & -J_Z/4 \end{bmatrix}. \quad (16)$$

Since  $\beta H_Z c \gg J_Z$ , the eigenvalues of (16) and their eigenstates are:

$$E_A = \beta H_Z c + J_Z/4, \quad | +1/2, +1/2 \rangle, \quad (17)$$

$$E_B = -\beta H_Z c + J_Z/4, \quad | -1/2, -1/2 \rangle, \quad (18)$$

$$E_C = -J_Z/4 + (J_X + J_Y)/4, \quad \{ | +1/2, -1/2 \rangle + | -1/2, +1/2 \rangle \} / \sqrt{2}, \quad (19)$$

$$E_D = -J_Z/4 - (J_X + J_Y)/4, \quad \{ | +1/2, -1/2 \rangle - | -1/2, +1/2 \rangle \} / \sqrt{2}. \quad (20)$$

The first three states  $A$ ,  $B$ , and  $C$  are triplet ( $S=1$ ), while the last state  $D$  is singlet ( $S=0$ ). Resonance occurs between  $A$  and  $C$  and between  $B$  and  $C$  for which  $\Delta m_S = \pm 1$ . From the resonance conditions  $h\nu = E_A - E_C$  and  $h\nu = E_C - E_B$ , we obtain the following resonance magnetic fields:

$$H_Z = h\nu/\beta c - (2J_Z - J_X - J_Y)/4\beta c, \quad (21)$$

$$H_Z = h\nu/\beta c + (2J_Z - J_X - J_Y)/4\beta c. \quad (22)$$

The tensor  $\mathbf{J}$  can be divided into an isotropic part  $J_0$  and an anisotropic part  $J'$  [ $J_0$  has no effect on (21) and (22) and  $J'$  corresponds to  $\mathbf{D}$  in (2)]. In the diagonal representation of  $\mathbf{J}$ , its diagonal components are  $J_X = J_0 + J'_X$ ,  $J_Y = J_0 + J'_Y$ , and  $J_Z = J_0 + J'_Z$ . If these are substituted into (21) and (22) and  $J'_X + J'_Y + J'_Z = 0$  is taken into account, we obtain

$$H_Z = h\nu/\beta c - 3J'_Z/4\beta c, \quad (23)$$

$$H_Z = h\nu/\beta c + 3J'_Z/4\beta c. \quad (24)$$

When  $\mathbf{H}$  is parallel to  $X$ , (14) is reduced to

$$\begin{aligned} H = & \beta H_X a (S_X^{(1)} + S_X^{(2)}) + J_X S_X^{(1)} S_X^{(2)} + \frac{1}{4} (J_Y - J_X) S_+^{(1)} S_+^{(2)} \\ & + \frac{1}{4} (J_Y + J_X) S_+^{(1)} S_-^{(2)} \\ & + \frac{1}{4} (J_Y + J_X) S_-^{(1)} S_+^{(2)} + \frac{1}{4} (J_Y - J_X) S_-^{(1)} S_-^{(2)} \end{aligned} \quad (25)$$

if  $X$  is taken to be the quantization axis, where the terms containing  $d$  in (14) are neglected because  $d$  is about three orders of magnitude as small as  $a$ ,  $b$ , and  $c$  as estimated from (9)–(12) and Table II. The resonance magnetic fields obtained from (25) are

$$H_X = h\nu/\beta a - 3J'_Z/4\beta a, \quad (26)$$

$$H_X = h\nu/\beta a + 3J'_Z/4\beta a. \quad (27)$$

Similarly, when  $\mathbf{H}$  is parallel to  $Y$ , we obtain the following resonance magnetic fields:

$$H_Y = h\nu/\beta b - 3J'_Z/4\beta b, \quad (28)$$

$$H_Y = h\nu/\beta b + 3J'_Z/4\beta b. \quad (29)$$

To summarize, if our assumption that the “ $X$ ” spectrum is due to the pair of two Ti interstitials shown in Fig. 4 is correct, the observed “ $X$ ” spectrum should satisfy (23), (24), and (26)–(29). Since  $h\nu/\beta c$ ,  $h\nu/\beta a$ , and  $h\nu/\beta b$  in these equations are the resonance magnetic fields of the “ $A$ ” spectrum, the two branches of the “ $X$ ” spectrum should always appear on the both sides of the “ $A$ ” spectrum with the same separation. This is qualita-

tively satisfied as we see in Figs. 2(a) and 2(b). Quantitatively, a deviation from this expectation is observed; the deviation is 18%, 0.2%, and 7% in the  $Z$ ,  $Y$ , and  $X$  directions, respectively, where the deviation is defined to be the shift of the center of the two branches of the “ $X$ ” spectrum from the resonance magnetic field of the “ $A$ ” spectrum divided by the separation of the two branches. The deviations can be interpreted as follows.

In the argument given above, we have assumed that all the principal values of the  $\underline{g}$  tensor of the isolated Ti interstitial,  $g_\xi$ ,  $g_\eta$ , and  $g_\zeta$ , are conserved even if another Ti interstitial approaches it to form the pair Ti(1)-Ti(2) in Fig. 4. However, if we consider one of the Ti interstitials, Ti(1), the orbitals of its paramagnetic electron about the  $\zeta(1)$  and  $\xi(1)$  axes [these axes are perpendicular or nearly perpendicular to the Ti(1)-Ti(2) axis] are affected by the existence of Ti(2), although the orbital about the  $\eta(1)$  axis [this axis is nearly parallel to the Ti(1)-Ti(2) axis] is not appreciably affected. Because of this,  $g_{\xi(1)}^{(1)}$  and  $g_{\zeta(1)}^{(1)}$  are actually different from  $g_\xi$  and  $g_\zeta$ , whereas  $g_{\eta(1)}^{(1)}$  is almost the same as  $g_\eta$ . We can say the same thing for  $g_{\xi(2)}^{(2)}$ ,  $g_{\zeta(2)}^{(2)}$ , and  $g_{\eta(2)}^{(2)}$ . Namely, (4) and (6) are not necessarily good approximations, although (5) is still a good approximation. Therefore, we must rewrite (9)–(12) as follows:

$$a = (g_\xi + \Delta) \cos^2 \theta + g_\eta \sin^2 \theta, \quad (30)$$

$$b = (g_\xi + \Delta) \sin^2 \theta + g_\eta \cos^2 \theta, \quad (31)$$

$$c = g_\zeta + \Delta', \quad (32)$$

$$d = (g_\eta - g_\xi - \Delta) \sin \theta \cos \theta, \quad (33)$$

where  $\Delta$  and  $\Delta'$  are the above-mentioned changes in  $g_\xi$  and  $g_\zeta$ , respectively. Although  $\theta$  also changes, it causes only a small correction. If we compare (30), (31), and (32) with (9), (10), and (11), respectively, it is found that  $c$  is most strongly changed,  $b$  is essentially unchanged (note that  $\sin^2 \theta = 0.19$  is much smaller than  $\cos^2 \theta = 0.81$ ), and  $a$  is moderately changed (only one of the two terms is changed). Since  $c$ ,  $b$ , and  $a$  are contained in (23) and (24) for  $\mathbf{H} \parallel Z$ , (28) and (29) for  $\mathbf{H} \parallel Y$ , and (26) and (27) for  $\mathbf{H} \parallel X$ , respectively, the deviation of concern is largest in  $Z$  (18%), almost zero in  $Y$  (0.2%), and medium in  $X$  (7%).

The principal values of the  $\mathbf{D}$  tensor shown in Table II are about one order of magnitude as small as those usually observed in transition-metal complex salts.<sup>8</sup> This is consistent with our picture that the two paramagnetic electrons interact with each other with a considerably large distance of 3.25 Å.

In this way, the “ $X$ ” spectrum is successfully interpreted by the pair of Ti interstitials shown in Fig. 4. This is supported by other experimental results shown in Fig. 5, where the intensity of the “ $C$ ”, “ $X$ ”, and “ $W$ ” spectra are

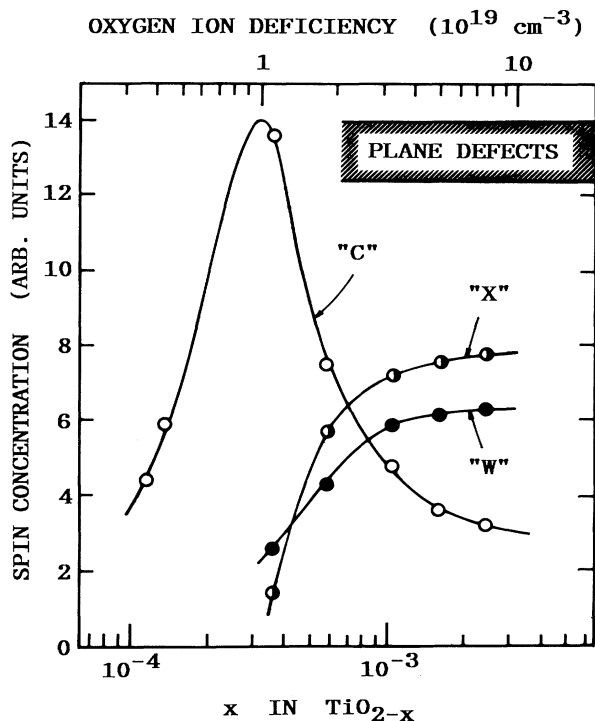


FIG. 5. Intensities of the "C," "X," and "W" spectra in a unit of spin concentration plotted against  $x$  in  $\text{TiO}_{2-x}$  (the measurements were made at 4.2 K); it is also shown that plane defects appear for  $x \geq 6 \times 10^{-3}$  [reproduced from a previous paper by one of the present authors (Ref. 1)].

plotted against  $x$  in  $\text{TiO}_{2-x}$ . As we see, as  $x$  increases, the intensity of the "C" spectrum due to the isolated Ti interstitials increases at first but decreases for  $x \geq 3 \times 10^{-4}$ . In accordance with the decrease, the "X" spectrum appears and increases in intensity. This is consistent with our interpretation that the "X" spectrum is caused by the pairing of the Ti interstitials.

### C. The "W" spectrum

The "W" spectrum was also found and named by Hasi-guti *et al.*<sup>10,11</sup> in their preliminary study. The "W" spectrum consists of four resonance lines and their resonance magnetic fields vary against the direction of the external magnetic field as shown in Figs. 6(a) and 6(b). As we see in Fig. 6(b), the "W" spectrum gives a single resonance line in the principal symmetry axis of  $\text{TiO}_2$ , [001], indicating that this spectrum is due to a single paramagnetic electron ( $S = 1/2$ ). Therefore, we shall analyze the "W" spectrum using (1). The principal axes and principal values of the  $g$  tensor determined from Figs. 6(a) and 6(b) are shown in Table III. An interesting characteristic of the "W" spectrum is that the principal axes of the  $g$  tensor in the (001) plane are deviated from the [100] and [010] crystal axes by a small angle of  $4.5^\circ$ . Any plausible point defects and simple defect complexes are inconsistent with this fact. Namely, the "W" spectrum is due to a pretty complicated defect.

TABLE III. Principal axes and principal values of the  $g$  tensor of the "W" spectrum.

Principal axis	Principal value
[001]	1.791
[100] $\pm 4.5^\circ$	2.053
[010] $\pm 4.5^\circ$	1.835

In conclusion, the "W" spectrum is analyzed to be due to a structural unit that constructs a plane defect. In fact, as studied by Yagi and Hasiguti<sup>12</sup> and indicated in Fig. 5,<sup>1</sup> {275} and {132} plane defects are observed by transmission electron microscopy in a region of  $x$  where the "W" spectrum appears.

According to Bursill, Hyde, and Philip,<sup>13</sup> a  $(hkl)$  plane defect in  $\text{TiO}_2$  can be constructed as

$$(hkl) = n(121) + m(011),$$

where  $n$  and  $m$  are integers and (121) and (011) represent a stacking fault and a phase boundary, respectively. The

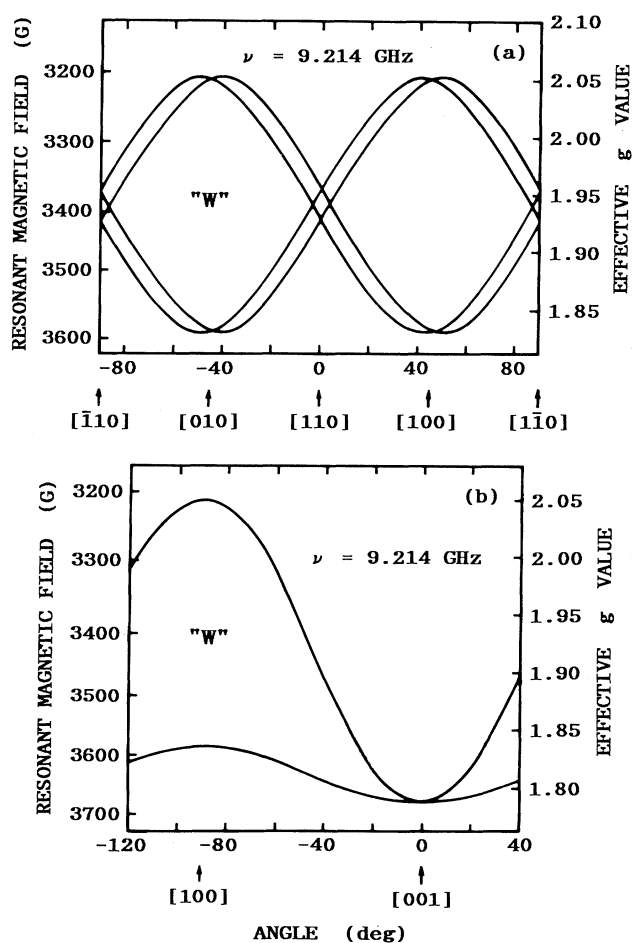


FIG. 6. Resonant magnetic fields of the "W" spectrum plotted against the direction of the external magnetic field; corresponding effective  $g$  values can be read from a scale on the right-hand side. The measurements were made at 4.2 K with an electromagnetic wave of 9.214 GHz.

(121) stacking fault is just the same as the (121) stacking fault in the Magneli phases with  $Ti_nO_{2n-1}$  already described. The (011) phase boundary will be described later. The (275) and (132) plane defects mentioned above are therefore constructed as

$$(275) = 2(121) + 3(011),$$

$$(132) = 1(121) + 1(011).$$

The (275) plane defect, for example, is illustrated in Figs. 7(a) and 7(b). In the figures, O ions are arranged in a close packed structure for simplicity; this is called the idealized  $TiO_2$  structure. Figures 7(a) and 7(b) represent two neighboring (001) atomic planes of the idealized  $TiO_2$  structure; by stacking these planes alternately, the idealized  $TiO_2$  structure is constructed. In the figures, the solid, broken, and dashed-dotted lines show the intersections of the (121) stacking fault, the (011) phase boundary, and the resultant (275) plane defect with the atomic planes, respectively. The deficiency of O ions is borne only by the (121) stacking fault.

We notice in Figs. 7(a) and 7(b) that there are pairs of Ti ions in the (121) stacking fault, i.e.,  $P-Q$  in Fig. 7(a) and  $P'-Q'$  in Fig. 7(b), although they are crystallographically equivalent. The origin of the "W" spectrum is attributed to this pair of Ti ions as will be discussed below in detail.

First, let us consider the principal axes of the  $g$  tensor shown in Table III. For this purpose, the Ti ion pair  $P-Q$  in Fig. 7(a) is redrawn in Fig. 8 for the real  $TiO_2$  struc-

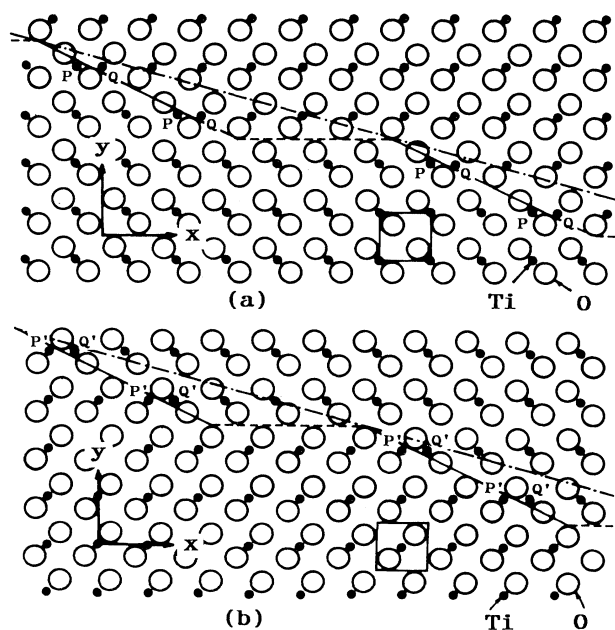


FIG. 7. Illustration of the (275) plane defect in  $TiO_{2-x}$  ( $x \approx 6 \times 10^{-3}$ ); O ions are arranged in a close packed structure for simplicity. (a) and (b) represent two neighboring (001) atomic planes and the solid, broken, and dashed-dotted lines show the intersections of a (121) stacking fault, a (011) phase boundary, and the resultant (275) plane defect with the atomic planes, respectively.

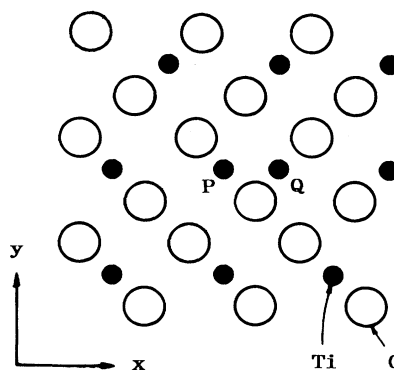


FIG. 8. Ti ion pair  $P-Q$  in Fig. 7(a) redrawn for the real  $TiO_2$  structure.

ture. Since the two Ti ions  $P$  and  $Q$  are arranged along  $[100]$ , one of the principal axes of the  $g$  tensor should be close to  $[100]$  and the other principal axes close to  $[010]$  and  $[001]$  which are perpendicular to  $[100]$ . A deviation from these axes is determined by the distortion of the arrangement of surrounding O ions from mirror symmetry about the (100) plane. As we see in Fig. 8, such distortion is small. In this way, the important characteristic of the "W" spectrum that the principal axes of the  $g$  tensor are in, or slightly deviated from  $[100]$  and  $[010]$ , can be interpreted.

As we can count easily, the Ti ion pair including surrounding O ions has sixteen crystallographically equivalent orientations. However, a half of them are the inversion of the rest half, which cannot be distinguished from each other by EPR. Furthermore, one of the principal axes of the  $g$  tensor coincides with the principal crystal axis  $[001]$ , so that the number of orientations distinguishable by EPR is four. This is consistent with the fact that the "W" spectrum consists of four resonance lines.

The principal values of the  $g$  tensor shown in Table III are also consistent with the Ti ion pair  $P-Q$  in Fig. 8. The paramagnetic electron of the Ti ion pair  $P-Q$  is represented by a linear combination of atomic orbitals of the two Ti ions  $P$  and  $Q$  arranged along  $[100]$ , so that the orbital should have strong axial symmetry about the  $[100]$  axis. We can therefore expect that the  $g$  tensor also has strong axial symmetry in a manner that the principal value of the  $g$  tensor in  $[100]$  (we neglect the small deviation of  $\pm 4.5^\circ$  which was discussed above) is largely different from those in  $[001]$  and  $[010]$  (which are perpendicular to  $[100]$ ), the latter two being close to each other. As we see in Table III, the principal value in  $[100]$  ( $\pm 4.5^\circ$ ) is certainly larger than those in  $[010]$  ( $\pm 4.5^\circ$ ) and  $[001]$  to a large extent; the latter two are almost equal.

An interesting thing seen in Table III is that the principal values of the  $g$  tensor are larger than the  $g$  value of a free electron,  $g_e (= 2.0023)$ , in  $[100] \pm 4.5^\circ$  but smaller than  $g_e$  in  $[010] \pm 4.5^\circ$  and  $[001]$ . The principal values are given by<sup>8</sup>

$$g_v = g_e - 2\lambda \sum_n \frac{\langle \phi_0 | L_v | \phi_n \rangle \langle \phi_n | L_v | \phi_0 \rangle}{E_n - E_0}, \quad (34)$$

where  $\nu$  represents one of the principal axes,  $\lambda$  the spin-orbit coupling constant,  $L_\nu$  the orbital momentum operator,  $E_0$  and  $E_n$  the energy levels of the paramagnetic electron and other filled and empty states, respectively, and  $|\phi_0\rangle$  and  $|\phi_n\rangle$  the wave functions of the paramagnetic electron and the filled and empty states, respectively, which can be written (in the present case) as

$$|\phi_0\rangle = C_0^P |\phi_P\rangle + C_0^Q |\phi_Q\rangle,$$

$$|\phi_n\rangle = C_n^P |\phi_P\rangle + C_n^Q |\phi_Q\rangle,$$

where  $|\phi_P\rangle$  and  $|\phi_Q\rangle$  are the atomic orbitals of the two Ti ions  $P$  and  $Q$  in Fig. 8.

If the paramagnetic electron at  $E_0$  interacts only with empty states at  $E_n$ 's above  $E_0$ , all the principal values of the  $\underline{g}$  tensor should be smaller than  $g_e$ , because the second term of (34) is negative in such a case. This is inconsistent with the experimental results mentioned above (Table III). Namely, at least one filled state must exist at an  $E_n$  below  $E_0$ , the  $E_n$  being not far from  $E_0$ . This means that there are at least two valence electrons in the Ti ion pair  $P$ - $Q$ , in addition to the paramagnetic electron of concern, and they make a covalent bond with uniparallel spins. The existence of such covalent bond electrons has already been inferred by Goodenough<sup>14</sup> in his argument on the Magneli phases. We have been able to verify his inference experimentally.

When the concentration of the Ti ion pair  $P$ - $Q$  is large as in the specimen for which Fig. 1 was measured, no hyperfine structure due to a nuclear spin of Ti,  $I$ , is observed because of exchange narrowing. However, when the concentration is small enough, or  $x$  in  $\text{TiO}_{2-x}$  is smaller than  $3 \times 10^{-4}$ , a hyperfine structure is observed as shown in Fig. 9, which was measured for a specimen with  $x = 3 \times 10^{-4}$ . There are two isotopes of Ti with a nuclear spin, i.e.,  $^{47}\text{Ti}$  and  $^{49}\text{Ti}$  with  $I = 5/2$  and  $7/2$ , respectively; their natural abundances are 7.32 and 5.46%, respectively, the nuclear magnetic moments of  $^{47}\text{Ti}$  and  $^{49}\text{Ti}$  are  $-0.7873$  and  $-1.102\beta_N$ , respectively,  $\beta_N$  being the nuclear magneton. The ratio of the former to the latter, 0.715, accidentally coincides with the ratio of  $5/2$  to  $7/5$ , 0.715. Therefore, eight  $[2(7/2)+1]$  resonance lines appear and the two lines at the both ends are weaker than the other lines, as we see in Fig. 9 (although Fig. 9 shows that the paramagnetic electron interacts only with a single Ti nuclear spin, this is not inconsistent with the Ti ion pair  $P$ - $Q$  because the probability that the both Ti ions have a nuclear spin is only 1.64%). The coupling constant  $A$  in the hyperfine interaction  $\mathbf{AI} \cdot \mathbf{S}$  (the notations have the usual meanings) is measured to be  $4.9 \times 10^{-4} \text{ cm}^{-1}$  from Fig. 9, which is about one order of magnitude as small as usual values.<sup>8</sup> This is consistent with the picture mentioned above that the paramagnetic electron is weakly bound to the Ti ion pair  $P$ - $Q$  after the two covalent bond electrons are trapped.

#### IV. SUMMARY

The atomic and electronic structures of lattice defects created in oxygen-deficient rutile  $\text{TiO}_{2-x}$  were studied in

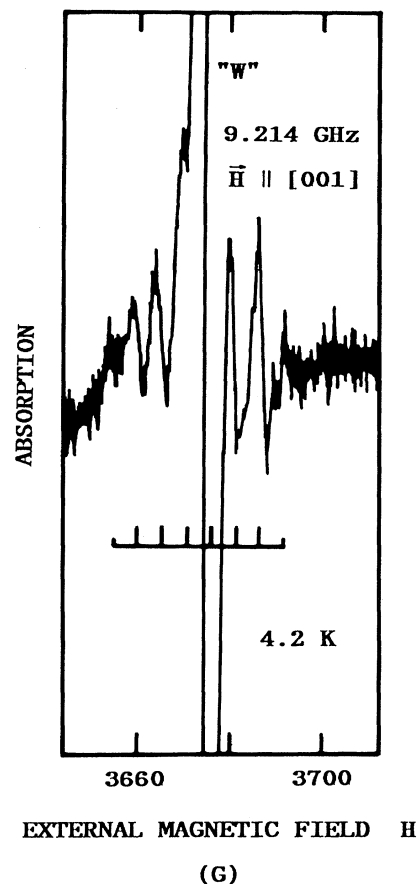


FIG. 9. "W" spectrum measured for  $\text{TiO}_{2-x}$  with  $x = 3 \times 10^{-3}$  (the conditions of measurements were the same as those in Fig. 1). A hyperfine structure is observed as indicated by vertical lines.

a region of  $1 \times 10^{-4} \lesssim x \lesssim 3 \times 10^{-3}$  by means of EPR. For small  $x$  ( $\lesssim 3 \times 10^{-4}$ ), the main lattice defects are Ti interstitials with a single paramagnetic electron ( $S = 1/2$ ). As  $x$  increases ( $\gtrsim 4 \times 10^{-4}$ ), the Ti interstitials interact with each other resulting in Ti interstitial pairs with two paramagnetic electrons ( $S = 1$ ) whose Ti-Ti distance and orientation are  $3.25 \text{ \AA}$  and  $\langle 110 \rangle$ , respectively. In the same region of  $x$ , a considerable part of Ti interstitials are orderly arranged in cooperation with an O deficit, resulting in  $\{121\}$  plane defects. The  $(121)$  plane defect contains Ti ion pairs whose Ti-Ti orientation is  $\langle 110 \rangle$ . This Ti ion pair has two covalent bond electrons and an additional paramagnetic electron ( $S = \frac{1}{2}$ ).

#### ACKNOWLEDGMENTS

We are very grateful to S. Takahashi for his assistance in EPR experiments. We also want to thank E. Yagi and E. Iguchi for many discussions.

- <sup>1</sup>For a review of previous studies on lattice defects in rutile (TiO<sub>2</sub>), see R. R. Hasiguti, *Ann. Rev. Mater. Sci.* **2**, 69 (1972).
- <sup>2</sup>R. R. Hasiguti, in *Proceedings of the International Conference on Radiation Physics of Semiconductors and Related Materials*, Tbilisi, USSR, September 1979, edited by G. P. Kekelidze and V. I. Shakhovtsov (Tbilisi State University Press, Tbilisi, 1980), p. 225.
- <sup>3</sup>S. Anderson, B. Collen, U. Kuylenstierna, and A. Magneli, *Acta Chem. Scand.* **11**, 1641 (1957).
- <sup>4</sup>P. F. Chester, *J. Appl. Phys.* **32**, 2233 (1961).
- <sup>5</sup>P. F. Chester (unpublished).
- <sup>6</sup>E. Yagi, A. Koyama, H. Sakairi, and R. R. Hasiguti, *J. Phys. Soc. Jpn.* **42**, 939 (1977); in *Radiation Effects in Semiconductors 1976*, edited by N. B. Uril and J. W. Corbett, IOP Conf. Proc. No. 31 (Institute of Physics, London, 1977), p. 485.
- <sup>7</sup>P. I. Kingsbury, Jr., W. D. Ohlsen, and O. W. Johnson, *Phys. Rev.* **175**, 1091 (1968).
- <sup>8</sup>G. E. Pake, *Paramagnetic Resonance* (Benjamin, New York, 1962).
- <sup>9</sup>R. R. Hasiguti, E. Yagi, and M. Aono, *Radiat. Eff.* **4**, 137 (1970).
- <sup>10</sup>R. R. Hasiguti, E. Iguchi, and S. Takahashi, in *Proceedings of the 9th International Conference on Physics of Semiconductors*, Moscow, USSR, 1968 (Nauka, Leningrad, 1968), Vol. 2, p. 1142.
- <sup>11</sup>R. R. Hasiguti, E. Iguchi, and S. Takahashi, *Ann. Rep. Nat. Res. Inst. Metals, Japan* **13** (1), 12 (1970).
- <sup>12</sup>E. Yagi and R. R. Hasiguti, in *Lattice Defects in Semiconductors* (Institute of Physics, London, 1974), p. 359; *J. Phys. Soc. Jpn.* **43**, 1998 (1977).
- <sup>13</sup>L. A. Bursill, B. G. Hyde, and D. H. Philp, *Philos. Mag.* **32**, 1501 (1971).
- <sup>14</sup>J. B. Goodenough, *Czech. J. Phys. B* **17**, 304 (1967).